CHARACTERISTICS AND CYTOTOXICITY OF MAGNETIC NANO PARTICLES ON BREAST CANCER CELLS

S. KANAGESAN[a*], M. HASHIM[a], S. TAMILSELVAN[b], N.B. ALITHEEN[b], I. ISMAIL[a], M.A.N. ISMAIL[a], G. BAHMANROKH[a].,M.M.RAHMAN[c]
[a]*Materials Synthesis and Characterization Laboratory (MSCL), Institute of Advanced Technology (ITMA), Universiti PutraMalaysia,43400 Serdang, Selangor, Malaysia*
[b]*Department of Cell and Molecular Biology, Faculty of Biotechnology and Biomolecular Sciences, University Putra Malaysia, 43400 Serdang, Selangor, Malaysia.*
[c]*Materials Processing and Technology Laboratory (MPTL), Institute of Advanced Technology (ITMA), Universiti PutraMalaysia,43400 Serdang, Selangor, Malaysia*

We report the results of our attempt to reveal the effect of exposing breast cancer cells to selected magnetic nanoparticles. Thus, fine spherical nanoparticles of magnesium ferrite were synthesized by the sol-gel self-combustion method. Their phase composition, morphology, and magnetic properties were determined. A cytotoxicity test was performed on human breast cancer cell lines with various $MgFe_2O_4$ concentrations ranging from (25 μg/ml) to (800 μg/ml). The results of our studies reveal the biocompatibility of magnesium ferrite nanoparticles. Magnesium ferrite nanoparticles induced cell death in a dose dependent manner and promise to be a potential candidate for bio-applications such as drug delivery, magnetic resonance imaging and magnetic hyperthermia.

(Received August 27, 2013; Accepted April 30, 2014)

Keywords: Nano particles; Magnetism; Apoptosis; Breast cancer; Cytotoxicity

1. Introduction

Spinel ferrites with the chemical formula MFe_2O_4 (where M=Ni, CO, Mn, Mg, Zn) have attracted the attention of researchers in the last three decades because of their exclusive magnetic properties. They have a wide range of practical applications in the design of electronic circuits, high frequency devices and high density recording [1, 2]. $MgFe_2O_4$, being an important spinel ferrite, is also widely reported in the literature for its applications in various fields [3, 4, 5]. They are used as catalysts [8], gas sensing [9], sensors [10, 11], magnetic applications [12] hyperthermia [13] and also in anode materials for lithium ion batteries [14]. Nano-sized particles have been explored in many biological applications including drug and gene delivery vehicles [21, 22]. Due to the chemical stability and magnetic properties, ferrite nanoparticles have been widely considered for magnetic resonance imaging, magnetic extraction and targeted drug delivery [23, 24]. Nanoparticles of a ferrite can be synthesized by a number of methods such as conventional ceramic method [15], hydrothermal [16], micro emulsion method [17] sol gel method [18], citrate gel process [19], Co-precipitation [20], etc. Different methods of synthesis processes produce various microstructures, particle size or both with varied physical properties. Due to the high diffusibility of Mg^{2+} ions the cation distribution in the magnesium ferrite crystal lattice sites is very sensitive to heat treatment temperature [6, 7].

*Corresponding author: kanagu1980@gmail.com

In this work, $MgFe_2O_4$ nano powder is synthesized by the sol-gel self-combustion method involving lower-than-conventional heat treatment temperatures. The reduction of particle size from microns to nanometers influences the physicochemical properties of the ferrite nanoparticles based on size and surface effects.

In evaluating the potential of these nanoparticles for commercial applications and clinical adaptation, as toxicity of these nanoparticles is a critical factor, the cytotoxicity effect of these nanoparticles is screened and reported in this paper. In the literature, only a little information is available about the potent cytotoxicity of magnesium ferrite nanoparticles at cellular and molecular level. The cytotoxicity of various ferrite particles were analyzed by Kim et. al. [25] with the MTT (3-[4,5-dimethylthiazol-2-yl]- 2,5-diphenyltetrazolium bromide) assay and the agar overlay method.

They found that ferrite nanoparticles are safe at low concentrations and the normal tissues are not damaged. In another study, Sun et al investigated the cytotoxicity of several metal oxide nanoparticles on human cardiac microvascular endothelial cells and found that cytotoxicity was effective at high ferrite concentrations [26]. Furthermore, it has also been reported that magnesium based nanoparticles were successfully employed in tumor treatment [27]. Though many groups have investigated the acute cytotoxicity of various magnetic nanoparticles, to the best of our knowledge, the cytotoxicity of magnesium ferrite nanoparticles on 4T1 murine breast cancer cell line was not yet analyzed.

In the present work, sol-gel combustion-synthesized nanoparticles were characterized by TG/DSC (thermo gravimetric/differential scanning colorimetry), XRD (X-ray diffraction), FTIR (Fouriear transform infra-red spectroscopy), FESEM (Field emission scanning electron microscope), VSM (vibrating sample magnetometer) and further the cytotoxicity was also analyzed for their potential biomedical applications.

2. Experimental techniques

2.1 Preparation of MgFe2O4 nanoparticles

AR grade magnesium nitrate, ferric nitrate and citric acid were purchased from aldrich chemicals. Magnesium nitrate and ferric nitrate in the molar ratio of 1:2, and citric acid in the ratio of 1:1 with nitrates were dissolved in a minimum amount of ethanol. A suitable amount of oleic acid was added to the solution. The solution was stirred for 4 h at room temperature and kept in a vacuum rotary evaporator at 60–80 °C to remove surplus water. The gel was heated at 150 °C in a hot air oven for 24 h. A brown color $MgFe_2O_4$ powder was obtained.

2.2 Characterization

X-ray diffraction pattern of the calcined powder sample was taken using a X-ray diffractometer (PANalytical X'pert pro) with CuKa radiation at 45 kV and 40 mA (k = 0.15406 nm) in a wide range of 2θ ($10° \leq 2\theta \leq 80°$). The microstructure observation of the specimen was performed using a Transmission electron microscope (JEM 3010 - JEOL) with an accelerating voltage of 200 kV. The magnetic characteristics of the specimen was measured at room temperature using a vibrating sample magnetometer.

2.3. MTT assay

The murine breast cancer cells 4T1 were procured from ATCC and the cells were maintained and propagated in 90% RPMI medium containing 10% fetal bovine serum (FBS) and 1% penicillin/streptomycin. The 4T1 cells were transferred to 96 well plates and incubated for 24 h prior to adding magnesium ferrite nanoparticles. The processed $MgFe_2O_4$ powder nanoparticles were introduced with various concentrations and the plate was incubated for 24 h. MTT (5mg) was dissolved in 1 ml of phosphate-buffered saline and each well was introduced with 25 µl of the MTT solution and wrapped with aluminum foil and incubated at 37 ^oC for 4 h. After the time

period, 200 µl of dimethyl sulfoxide was used to replace the solution in containing media, unbound MTT and dead cells. The plates were mixed well and the optical density was observed using a micro plate reader at 575 nm. The experiment was performed in triplicates and the results were expressed as the percentage proliferation with respect to vehicle-treated cells.

2.4. Quantification of apoptosis

The cell death of 4T1 cells induced by $MgFe_2O_4$ was analyzed using propidium iodide (PI) and acridine-orange (AO) double staining and observed under fluorescence microscope (Bio-Rad). Briefly, 4T1 cells were plated at a concentration of $1x10^6$ cell/ml in a 25 ml culture flask. $MgFe_2O_4$ nanoparticles were incorporated into the flask at different concentrations. The treated 4T1 cells were incubated in 5% CO_2 at 37 °C for 24 h. The cells were centrifuged at 1000 rpm for 10 minutes and the cells were harvested. The cells were washed twice using PBS to remove the remaining media. The 4T1 cells were stained with 10µl of fluorescent dyes AO (10 µg/ml) and PI (10 µg/ml) and observed within 30 min under UV-fluorescence microscope. The experiments were performed three times individually and all measurements were attained in triplicate.

2.5. Assessment of lipid peroxidation

The 4T1 cells were plated at the concentration of $3x10^6$ and treated with different concentrations of magnesium ferrite nanoparticles for 24 h. The treated cells were lysed in a 260 µl solubilization buffer containing 10mM Tris, pH 7.4, 9 g/l NP40; 1 g/l SDS; 250 U/ml benzonase and spinned down at 20000g for 10 min at 4°C. An aliquot of 50µl was frozen at -20°C for protein measurements. The amount of 200µl of cell lysate or malondialdehyde standards were mixed with 10µl butylatedhydroxytoluene (50mg/ml ethanol) and 200 µl of orthophosphoric acid (0.2 mM). The reaction mixture was kept in ice for 30 min and centrifuged at 2000 g for 15 min. Afterwards, 25 µl of 2-thiobarbituric acid reagent (800 mg of 2-thiobarbituric acid dissolved in 50 ml of 0.1 M NaOH) was added to the supernatant and incubated at 90 °C for 45 min. Formed malondialdehyde equivalents TBARS (thiobarbituric acid reactive substances) were extracted and measured using a plate reader (BioRad) with excitation at 532 nm and 600 nm. For quantitative determination of TBARS, 200 µl of a malondialdehyde standard solution was used instead of cell lysate.

3. Results and discussion

3.1 Thermal analysis

TG/DSC curve of the gel is shown in Fig. 1. Once the temperature was increased from room temperature to 1200 °C, the sample lost about 31% of its initial weight as shown in the TG curve. The 31% of mass loss is due to the evaporation of absorbed water [28, 29]. Two endothermic peaks from 200 to 450°C are observed in DSC with 31% of weight loss in TG. They are due to the dehydration of OH group in NO3- constituent and the oxidation of complexes and the formation of semi-organic carbon metal/ metal oxide [30, 31]. The larger endothermic event with 20% of weight loss in the range of 450 to 550 °C represents the formation of equivalent metal oxides and the spinel phase. There is no weight loss observed above 600°C. This indicates the formation of pure $MgFe_2O_4$.

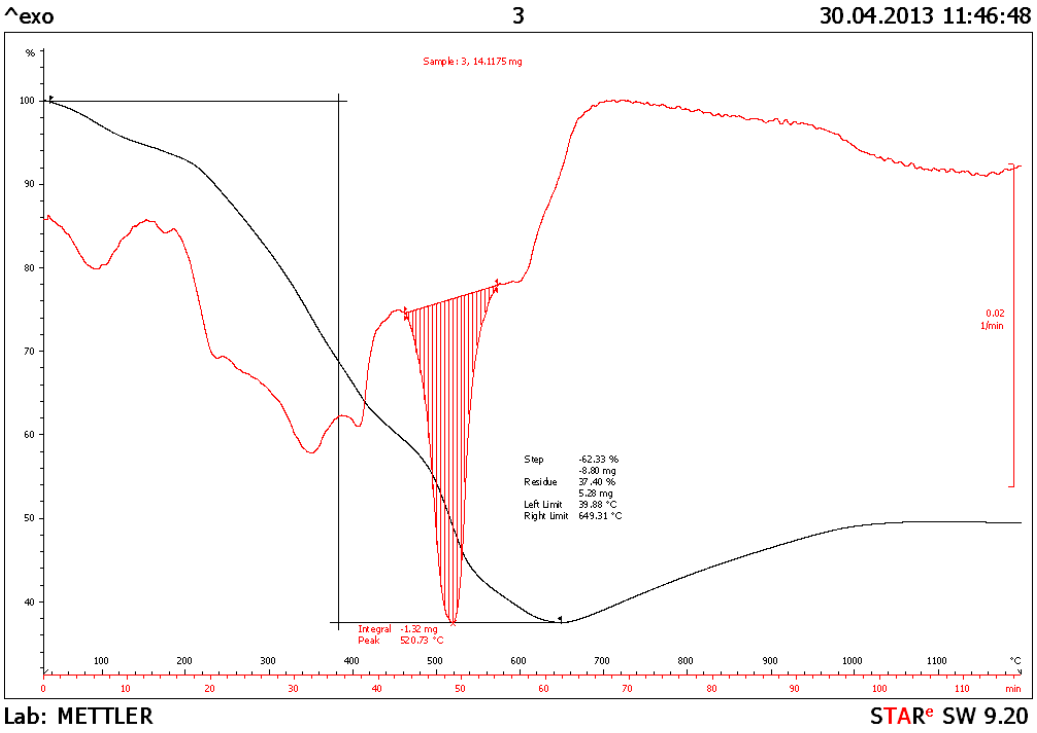

Fig. 1 TG/DSC curve of $MgFe_2O_4$ precursor powder

3.2 X-ray Diffraction (XRD) analysis

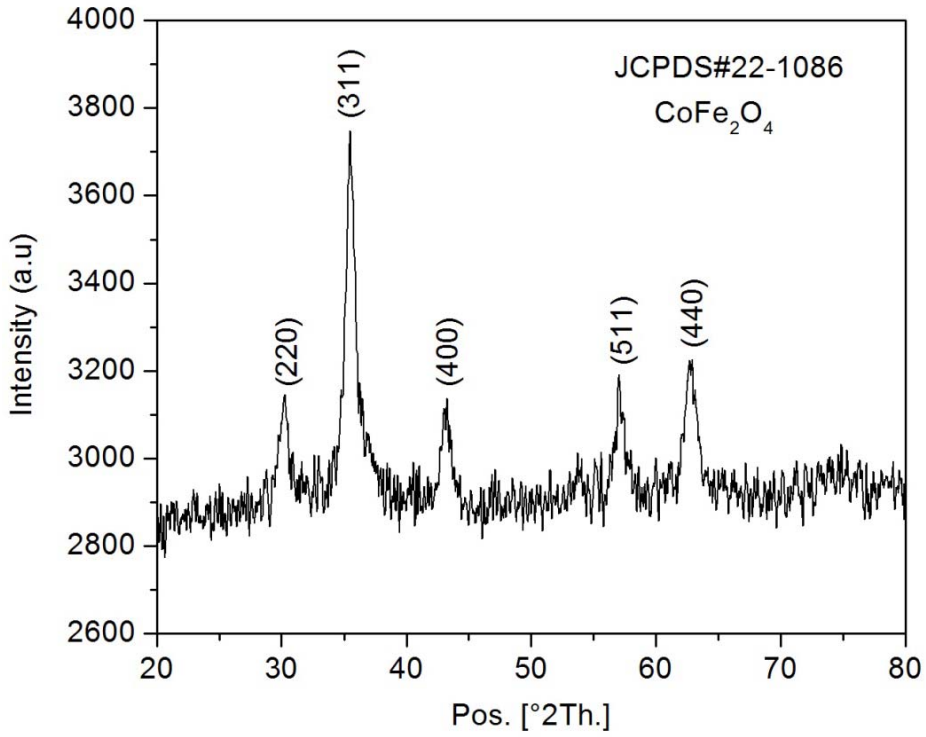

Fig. 2. XRD pattern of the $MgFe_2O_4$ nanopowder

The X-ray diffraction patterns of the calcined samples are shown in Fig. 2. The diffraction patterns observed at 2θ values of 0.88, 35.56, 43.09, 53.58, 57.21, 62.69 and 74.57 corresponds to (2 2 0), (3 1 1), (2 2 2), (4 0 0), (4 2 2), (3 3 3) and (4 4 0) planes, and match with the standard diffraction pattern card No; 22-1086. These patterns confirm that the samples are $MgFe_2O_4$ having a single-phase cubic spinel structure. The broad reflections noticed in the pattern indicate the nanocrystalline nature of the ferrites.

3.3 Particle size analysis

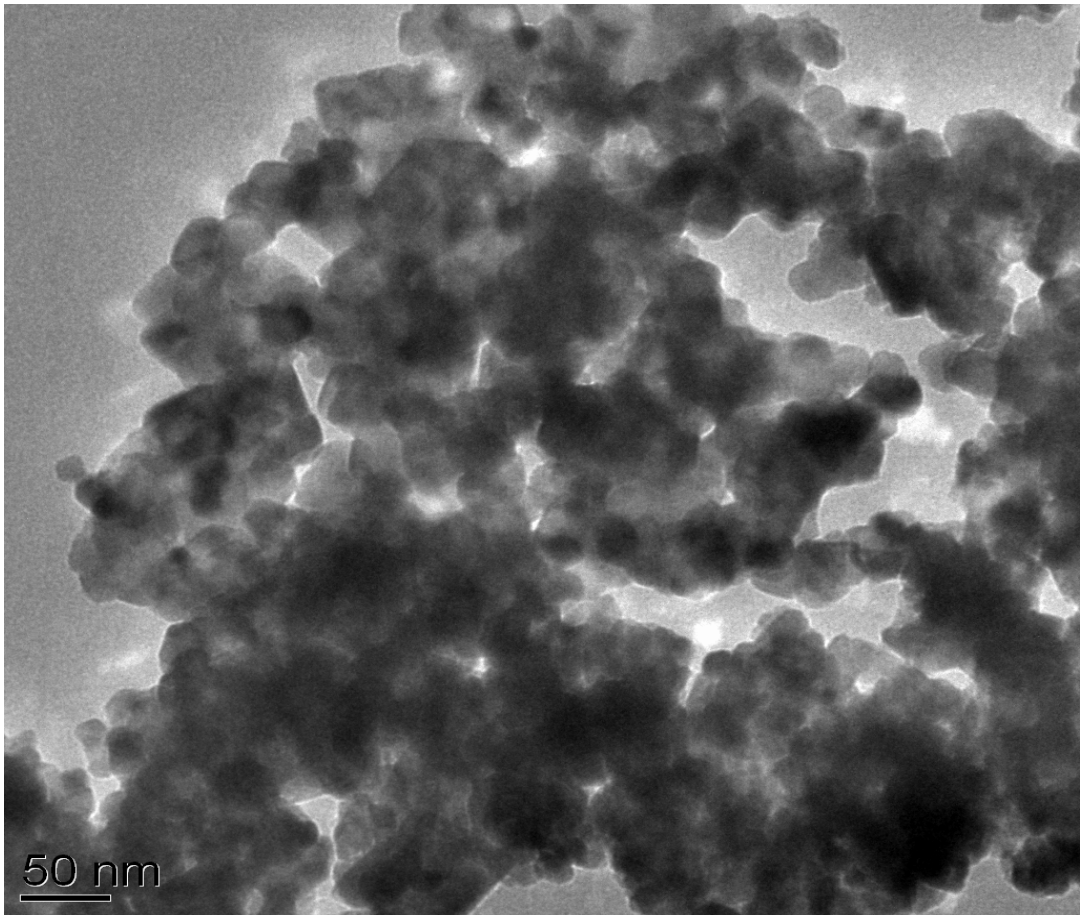

Fig. 3 : TEM micrograph of $MgFe_2O_4$ nanopowder

It is observed from transmission electron microscope images (Fig. 3), that most of the magnesium ferrite nanoparticles are spherical in shape with uniform particle size and are agglomerated. The mean diameter of the spherical particles is roughly about 25 nm.

3.4 Magnetic analysis

The magnetic hysteresis behavior of the $MgFe_2O_4$ nanopowder, studied at room temperature, is shown in Fig. 4. The hysteresis loop displays a low value of coercivity and a high value of saturation magnetization. Generally such observation occurs in soft ferrite materials like $MgFe_2O_4$, $NiFe_2O_4$, $ZnFe_2O_4$ ferrites. This compound exhibits ferromagnetic behavior at room temperature. It can be seen that the maximum saturation magnetization of 24.50 emu/g corresponds to the value of intrinsic coercivity Hc (124.77 Gauss). The saturation magnetization (Ms) value is less than that of bulk $MgFe_2O_4$ [32, 33]. This saturation value is almost 25% less than that of bulk value (33.4 emu g−1). The magnetization value depends on shape, crystallinity, preparation temperature, grain size, and the structure etc. [34-36]. The reduction of Ms may be due to the surface structural distortions and spin canting existing in the whole volume of the

nanoparticles. The different cation distributions in magnesium ferrite may have also reduced its Ms value compared to their bulk counterparts [37-39].

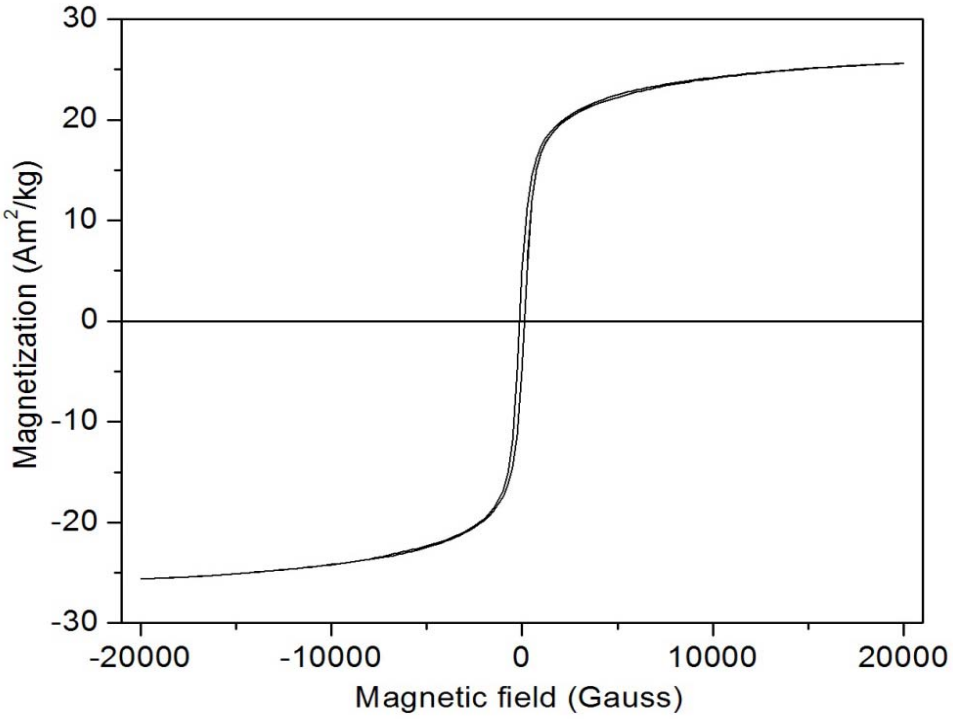

Fig. 4: Hysteresis loop of $MgFe_2O_4$ nanopowder

3.5. Cytotoxicity analysis

The 4T1 murine breast cancer cells were exposed to different concentrations of $MgFe_2O_4$ nanoparticles such as 25, 50, 100, 200, 400 and 800 µg/ml for 24h and the cytotoxicity was analyzed by MTT assays. The cytotoxicity of the ferrites was observed in a dose-dependent fashion with the increase in concentration of nanoparticles. The cell viability was significantly reduced to 92%, 91%, 88%, 69%, 47% and 31% for the concentrations of 25, 50, 100, 200, 400 and 800 µg/ml respectively ($p<0.05$ for each; Fig. 5). The concomitant observations made by other researchers demonstrated that magnesium nanoparticles exhibited toxicity at only high concentrations [40, 41]. The 4T1 cells treated with diverse concentrations of the $MgFe_2O_4$ nanoparticle were examined by fluorescence microscopy after AO/PI staining to characterize the $MgFe_2O_4$ nanoparticle-induced apoptosis. The morphological changes including cell shrinkage, condensed and fragmented chromatin are associated with apoptotic cell death [42]. As seen in Fig. 6, control cells did not show any apoptotic bodies after AO/PI staining. The cells treated with increasing concentrations of $MgFe_2O_4$ nanoparticle displayed a progressive accumulation of the apoptotic bodies in a dose dependent manner.

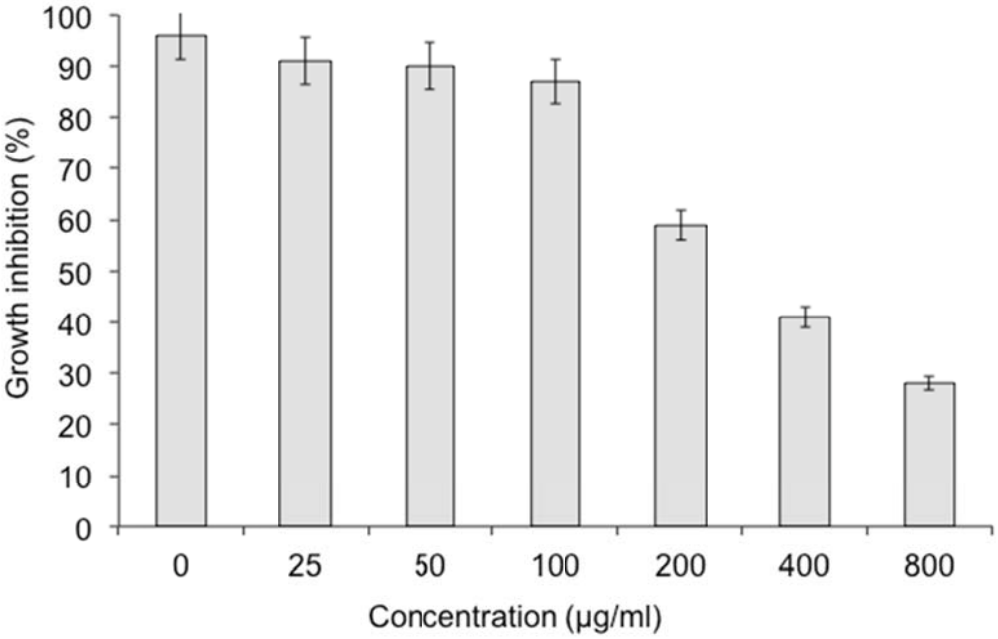

Fig. 5. Effect of $MgFe_2O_4$ on growth of murine breast cancer cell lines 4T1. Cells are seeded in 96-well plates and incubated with different concentrations of $MgFe_2O_4$ and noted after 24 h maintaining at 37 °C. Cell viabilities are determined by 3-(4,5-dimethylthiazol-2-yl)-2,5-diphenyl tetrazolium bromide (MTT) assay. Data points are presented as means ± SD of triplicate experiments.

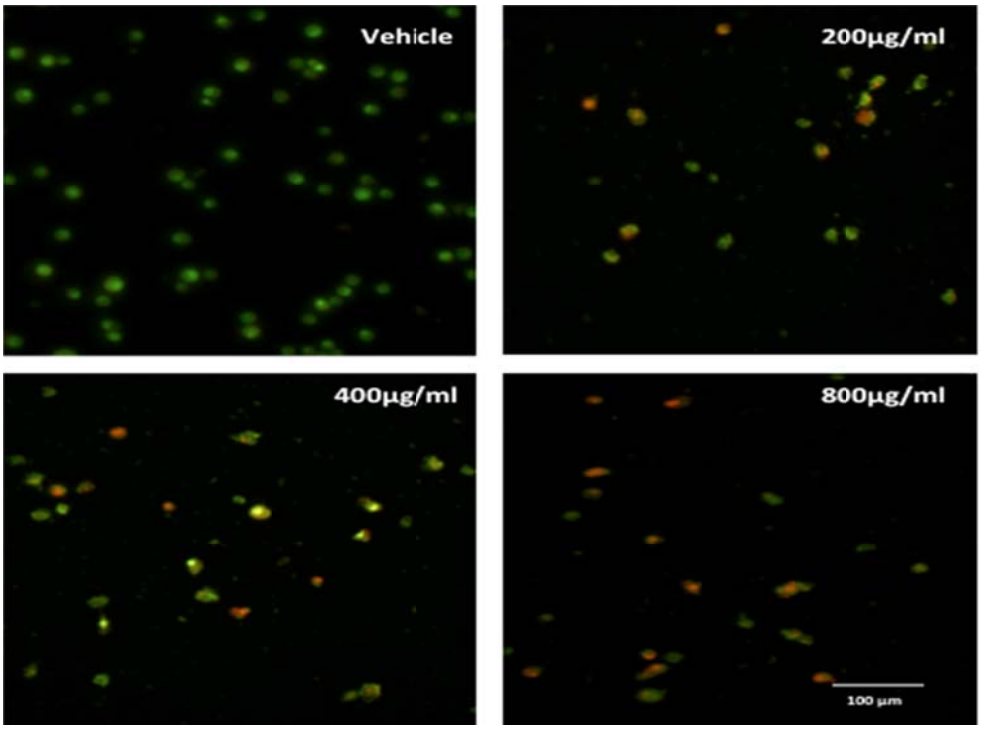

Fig. 6. Morphological assessment of 4T1 cells stained with acridine orange (green) and propidium iodine (red). Cells are incubated with or without $MgFe_2O_4$ at various concentrations for 24 h. Cells with intact membrane and stained green indicate viable cells; cells that are stained orange represent secondary necrotic or late apoptotic cells containing fragmented DNA (Magnification 100x, scale bar 20µm).

The influence of $MgFe_2O_4$ nanoparticles to induce oxidative stress was evaluated by determining the lipid peroxidation levels in 4T1 cells. $MgFe_2O_4$ nanoparticles significantly induced lipid peroxidation by 3 fold of the control in a dose dependent manner (Fig. 7). These results confirmed that $MgFe_2O_4$ nanoparticles at high concentrations induced oxidative stress in 4T1 cells by inducing the oxidants. Oxidative stress has been proposed as a common mechanism of cell damage induced by many types of nanoparticles [43-45].

For example, iron-based nanoparticles produced toxicity to biological systems by generating ROS [46-48] and it has been suggested to be signaling molecules for the initiation and execution of the apoptotic death program [49, 50]. To the best of our knowledge, there are only few sources of information available on the *in vitro* cytotoxicity of $MgFe_2O_4$ nanoparticles. We demonstrated the simultaneous visualization of viable, necrotic and apoptotic cells in treated and untreated 4T1 cells suggesting that $MgFe_2O_4$ nanoparticles induce apoptosis and necrosis at higher concentrations (400 µg/ml) in a dose dependent manner.

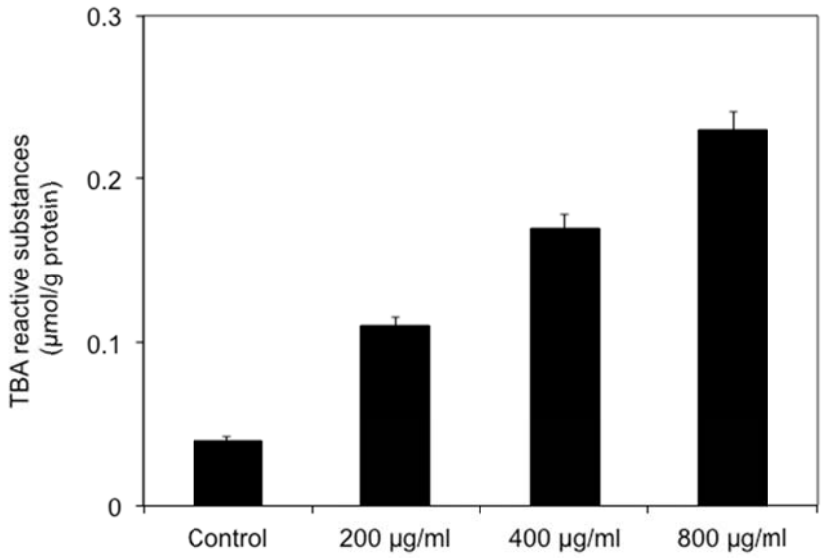

Fig. 7. Lipid peroxidation levels at different concentrations of $MgFe_2O_4$ nanoparticles.

4. Conclusions

The nanocrystalline $MgFe_2O_4$ have been synthesized by the sol-gel self-combustion route. The XRD patterns show the formation of single-phase cubic spinel structure. The particle sizes are controlled and the average particle size is about 25 nm. Our findings demonstrate the cytotoxicity of $MgFe_2O_4$ nanoparticles towards cancerous cells. $MgFe_2O_4$ nanoparticles enhances lipid peroxidation suggesting the active role of reactive oxygen species in the toxicity mechanism. Such bio behavior of $MgFe_2O_4$ nanoparticles may be used for drug carriers in cancer chemotherapy.

References

[1] S. Verma, P.A. Joy, Y.B. Khollam, H.S. Potdar, S.B. Deshpande, Mater. Lett. **58**, 1092 (2004).
[2] X. Yang, J. Dong, Appl. Phys. Lett. **86**, 163105 (2005).
[3] A. Pradeep, P. Priyadharsini, G. Chandrasekaran, Journal of Magnetism and Magnetic Materials **320**, 2774 (2008).
[4] J. Chandradass, A- H. Jadhav, K- H. Kim, H. Kim, Journal of Alloys and Compounds **517**, 164 (2012).

[5] Smitha Thankachan, Sheena Xavier, Binu Jacob, E.M. Mohammed, Journal of Experimental Nano science, **8(**3), 347 (2013).
[6] V.B. Kawade, G.K. Bichile, K.M. Jadhav, Mater. Lett. **42**, 33 (2000).
[7] E.W. Gorter, Nature **165**, 798 (1950).
[8] G. Busca, E. Finocchio, V. Lorenzelli, M. Trombetta, S.A. Rossini J. Chem. Soc., Faraday Trans. **92**, 4687 (1996).
[9] Y.-L. Liu, Z.-M. Liu, Y. Yang, H.-F. Yang, G.-L. Shen, R.-Q. Yu, Sens. Actuators B **107**, 600 (2005).
[10] S. Darshane, I.S. Mulla, Mater. Chem. Phys. **119**, 319 (2010).
[11] P.P. Hankare, S.D. Jadhav, U.B. Sankpal, R.P. Patil, R. Sasikala, I.S. Mulla, J. Alloys Compd. **488**, 270 (2009).
[12] A. Goldman, Modern Ferrite Technology, Van Nostrand, New York, 1990.
[13] Y. Ichiyanagi, M. Kubota, S. Moritake, Y. Kanazawa, T. Yamada, T. Uehashi, J. Magn. Magn. Mater. **310**, 2378 (2007).
[14] N. Siva Kumar, S.R.P. Gnanakan, K. Karthikeyan, S. Amaresh, W.S. Yoon, G.J. Park, Y.S. Lee, J. Alloys Compd. **509**, 7038 (2011).
[15] F. Novelo, R. Valenzuela, Mater. Res. Bull. **30**, 335 (1995).
[16] U. Bhattacharya, V.S. Darshane, J. Mater. Chem. **3**, 299 (1993).
[17] H.H. Hamdeh, J.C. Ho, S.A. Oliver, R.J. Willey, G. Oliveri, G. Busca, J. Appl. Phys. **81**, 1851 (1997).
[18] P.G. Bercoff, H.R. Bertorello, J. Magn. Magn. Mater. **169**, 314 (1997).
[19] L. John Berchmans, R. Kalai Selvan, P.N. Selva Kumar, C.O. Augustin, Journal of Magnetism and Magnetic Materials **279**, 103 (2004).
[20] A. Goldman and A. M. Laing, J. Phys., 1976, 4, C1.
[21] M. Premanathan, K. Karthikeyan, K. Jeyasubramanian and G. Manivannan, Nanomedicine: Nanotechnology, Biology and Medicine **7,** 184 (2011).
[22] P. Sanpui, A. Chattopadhyay and S.-S. Ghosh, ACS Appl. Mater. Interfaces **3**, 218 (2011).
[23] U. Hafeli Scientific and Clinical Applications of Magnetic Carriers. Plenum Press: New York; 1997. p. 117.
[24] QA, Pankhurst, J Connolly, SK Jones, J. Dobson, J Phys D: Appl Phys; **36**, R167 (2003).
[25] D-H Kim, S-H Lee, K-N Kim, K-M Kim, I-B Shim, Y-K Lee, Journal of Magnetism and Magnetic Materials **293**, 320 (2005)
[26] J. Sun, S. Wang, D. Zhao, F. H. Hun, L. Weng and H. Liu, Cell Biol. Toxicol. **27**(333),22 (2011).
[27] D.-R. Di, Z.-Z. He, Z.-Q. Sun, J. Liu, Nanomedicine: Nanotechnology, Biology and Medicine, 2012, 1–9.
[28] S. Jesurani, S. Kanagesan, R. Velmurugan, T. Kalaivani, J Mater Sci: Mater Electron **23,** 668 (2012).
[29] S. Kanagesan, S. Jesurani, R. Velmurugan, M. Siva Kumar, C. Thirupathi, T. Kalaivani, J Mater Sci: Mater Electron **23**, 635 (2012)
[30] C.Y. Zhang, X.Q. Shen, J.X. Zhou, M.X. Jing, K. Cao, J. Sol-Gel. Sci. Technol. **42**, 95 (2007)
[31] P. Sivakumar, R. Ramesh, A. Ramanand, S. Ponnusamy, C. Muthamizhchelvan, J Mater Sci: Mater Electron **23**, 1011 (2012).
[32] A Franco Jr, M. S. Silva, J. Appl. Phys. **109**, 07B505(2011)
[33] V Sepelak, B Baabe, D Mienert, F J Litterst, K D Becker Scr. Mater. **48**, 961 (2006).
[34] S. Kanagesan, S. Jesurani, R. Velmurugan, S. Prabu, T. Kalaivani, J Mater Sci: Mater Electron **23**, 1511 (2012).
[35] Smitha Thankachan, Binu P Jacob, Sheena Xavier, E M Mohammed, Phys. Scr. **87,** 025701 (2013).
[36] S S Khot, N S Shinde, B P Ladgaonkar, B B Kale, S C Watawe Adv. Appl. Sci. Res. **2**, 460 (2011)
[38] M M Rashad, R M Mohamed, H El-Shall, J. Mater. Proc. Technol. **198**, 139 (2008).
[39] N Bao, L Shen, Y Wang, P Padhan, A. Gupta J Am Chem Soc. **129,** 12374 (2007).
[40] M Rajendran, R C Pullar, A K Bhattacharya, D Das, S N Chintalapudi, C K Majumdar, J. Magn. Magn. Mater. **232**, 71 (2001).

[41] S. Ge, G. Wang, Y. Shen, Q. Zhang, D. Jia, H. Wang, Q. Dong, T. Yin, IET Nanobiotechnol. **5**, 36 (2011).
[42] G. F. Yang, X. H. Li, Z. Zhao, W. B. Wang, Acta. Pharmacol. Sin. **30**,1688 (2009).
[43] T.T. Mai, J.Y. Moon, Y.W. Song, P.Q. Viet, P.V. Phuc, J.M. Lee, T.H. Yi, M. Cho, S.K. Cho, Cancer Lett. **321**, 144 (2012).
[44] E.J. Park, J. Yi, K.H. Chung, D.Y. Ryu, J. Choi, K., Park, Toxicol. Lett. **180**, 222 (2008).
[45] E.J. Park, H. Kimb, Y. Kimb, , J. Yic, K. Choid, K. Park, Toxicology **275**, 65 (2010).
[46] V. Stone, K. Donaldson, Nanotoxicology: signs of stress. Nat. Nanotech. **1**, 23 (2006).
[47] A. Stroh, C. Zimmer, C. Gutzeit, M. Jakstadt, , F. Marschinke, , T. Jung, et al., Free Radic. Biol. Med. **36**, 976 (2004).
[48] Zhu, M.T., Wang, Y., Feng, W.Y., Wang, B., Wang, M., Ouyang, H., Chai, Z.F., J. Nanosci. Nanotechnol. **10**, 8584 (2010).
[49] Apopa, P.L., Qian, Y., Shao, R., Guo, N.L., Schwegler-Berry, D., Pacurari, M., et al., Part. Fibre Toxicol. **6**, 1 (2009).
[50] Ott, M., Gogvadze, V., Orrenius, S., Zhivotovsky, B., Apoptosis **12**, 913 (2007).
[51] Rana, S., Gallo, A., Srivastava, R.S., Misra, R.K.,. Acta Biomater. **3**, 233 (2007).